9-19-2021

Shallow Rupture Propagation of Pleistocene Earthquakes Along the Hurricane Fault, UT, Revealed by Hematite (U-Th)/He Thermochronometry and Textures

Madison P. Taylor
Utah State University

Alexis K. Ault
Utah State University

Margaret L. Odlum
University of Nevada, Las Vegas, margaret.odlum@unlv.edu

Dennis L. Newell
Utah State University

Repository Citation

Taylor, M. P., Ault, A. K., Odlum, M. L., Newell, D. L. (2021). Shallow Rupture Propagation of Pleistocene Earthquakes Along the Hurricane Fault, UT, Revealed by Hematite (U-Th)/He Thermochronometry and Textures. *Geophysical Research Letters, 48*(17), 1-11.
http://dx.doi.org/10.1029/2021GL094379`

Geophysical Research Letters®

RESEARCH LETTER
10.1029/2021GL094379

Key Points:

- Hematite textures and (U-Th)/He dates record mineralization and slip at ~0.65–0.36 Ma and ~300 m depth on the seismogenic Hurricane fault
- Comminution and hydrothermal fluids cause amorphization of hematite and adjacent host rock that weaken the fault during seismic slip
- Data demonstrate earthquake ruptures repeatedly propagate along localized slip surfaces in the shallow crust

Supporting Information:

Supporting Information may be found in the online version of this article.

Correspondence to:

A. K. Ault,
alexis.ault@usu.edu

Citation:

Taylor, M. P., Ault, A. K., Odlum, M. L., & Newell, D. L. (2021). Shallow rupture propagation of Pleistocene earthquakes along the Hurricane fault, UT, revealed by hematite (U-Th)/He thermochronometry and textures. *Geophysical Research Letters*, *48*, e2021GL094379. https://doi.org/10.1029/2021GL094379

Received 17 MAY 2021
Accepted 14 AUG 2021

Shallow Rupture Propagation of Pleistocene Earthquakes Along the Hurricane Fault, UT, Revealed by Hematite (U-Th)/He Thermochronometry and Textures

Madison P. Taylor[1], Alexis K. Ault[1], Margaret L. Odlum[1,2], and Dennis L. Newell[1]

[1]Department of Geosciences, Utah State University, Logan, UT, USA, [2]Department of Geoscience, University of Nevada, Las Vegas, Las Vegas, NV, USA

Abstract The material properties and distribution of faults above the seismogenic zone promote or inhibit earthquake rupture propagation. We document the depths and mechanics of fault slip along the seismically active Hurricane fault, UT, with scanning and transmission electron microscopy and hematite (U-Th)/He thermochronometry. Hematite occurs as mm-scale, striated patches on a >10 m^2 thin, mirror-like silica fault surface. Hematite textures include bulbous aggregates and cataclasite, overlain by crystalline Fe-oxide nanorods and an amorphous silica layer at the slip interface. Textures reflect mechanical, fluid, and heat-assisted amorphization of hematite and silica-rich host rock that weaken the fault and promote rupture propagation. Hematite (U-Th)/He dates document episodes of mineralization and fault slip between 0.65 and 0.36 Ma at ~300 m depth. Data illustrate that some earthquake ruptures repeatedly propagate along localized slip surfaces in the shallow crust and provide structural and material property constraints for in models of fault slip.

Plain Language Summary Earthquake ruptures can travel to the Earth's surface along discrete, large faults, or earthquake energy may be consumed in the shallow crust by the creation of small fault networks and fractured rock, which may reduce ground shaking intensity. Estimating earthquake hazards requires knowledge of subsurface material properties and how they change to promote or inhibit localized faulting. We investigate the Hurricane fault, UT, part of the Intermountain Seismic Belt or a north–south trending zone of recorded seismicity in the western US, which has the potential for large earthquakes (up to magnitude 7). We target hematite, an iron-oxide mineral, on a mirror-like, silica fault surface with microscopy and radiometric dating to document textural changes and the timing and depth of past fault slip. Nanoscale textures indicate the physical breakdown of hematite and surrounding rock, followed by the growth of new hematite and solidification of a silica surface layer, during an earthquake. Radioisotopic analyses capture hematite mineralization and fault slip 0.65–0.36 million years ago at shallow depths (~300 m). In this example, the combination of mechanical and hydrothermal processes weaken fault materials, leading to repeated propagation of earthquake ruptures toward the surface along a discrete fault.

1. Introduction

The shallow portions of fault zones accommodate the up-dip propagation of earthquake ruptures (Scholz, 2002). Forecasting earthquake hazards requires knowledge of slip distribution and the mechanical behavior of the shallow crust (Field et al., 2013; Nevitt et al., 2020; Petersen et al., 2015). Models for fault strength and predictions of rate-dependent frictional behavior with depth often depict the upper 3 km as an unconsolidated gouge or a voluminous bedrock zone(s) undergoing distributed deformation (e.g., Fagereng & Toy, 2011; Klinger et al., 2018; Sibson, 1983). Geodetic measurements indicate that a seismic slip deficit in the shallow crust may be explained by compliant zones of reduced elastic stiffness (Barbot et al., 2008) or elastoplasticity in off-fault damage zones (Kaneko & Fialko, 2011; Roten et al., 2017). However, fault growth, evolution, and structural maturity cause localization of on-fault deformation rather than creation of off-fault damage (Dolan & Haravitch, 2014). Paleoseismic trenches (Rockwell & Ben-Zion, 2007) and exhumed bedrock fault surfaces indicate deformation is localized even in the shallowest crust, and that structures are reactivated during recurring seismic events.

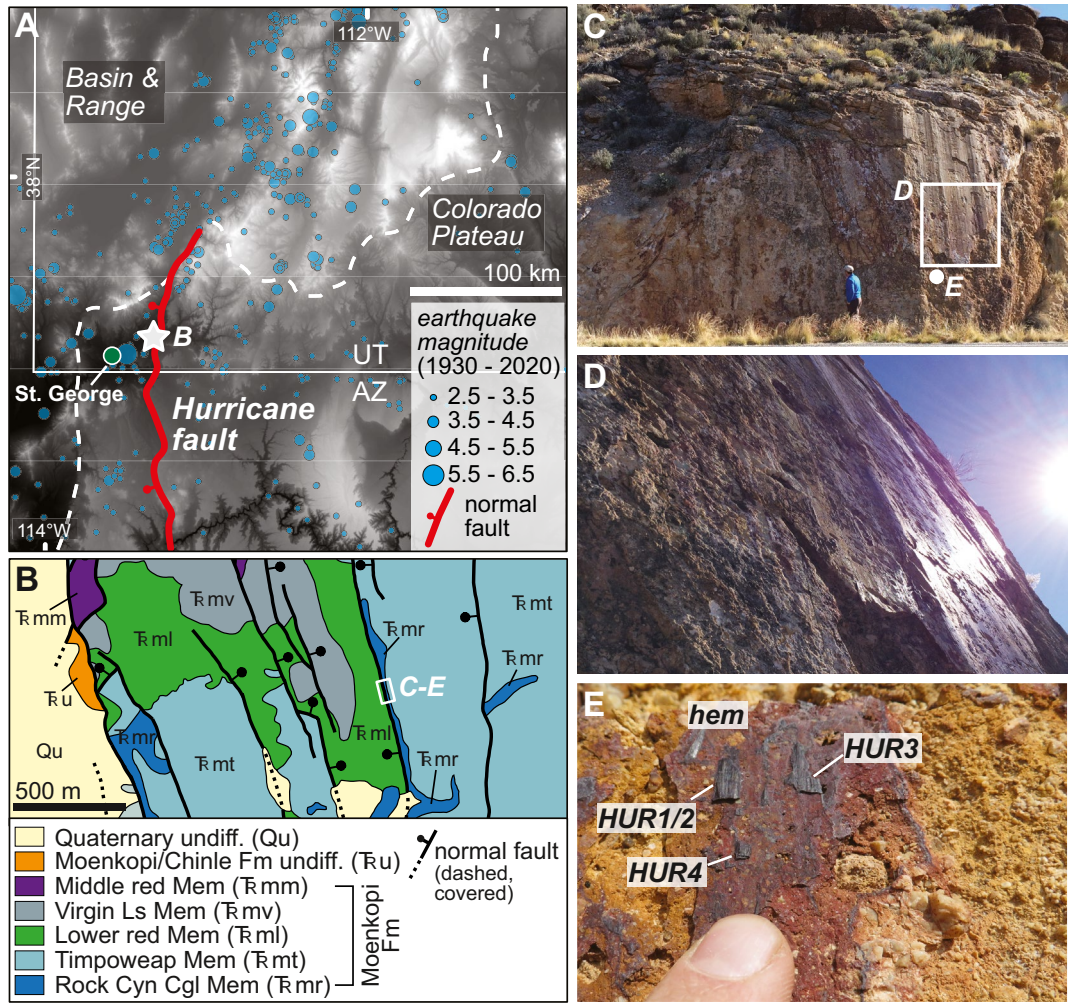

Figure 1. (a) Digital elevation model with the Hurricane fault and 1930–2020 earthquake catalog; blue circles scaled to earthquake magnitude. White star denotes study area. (b) Simplified geologic map modified from Biek (2003). White box is (c–e) location. (c–d) Field photographs of targeted, mirrored fault surface; (e) hematite patches.

Above the seismogenic zone (<3 km), frictional and fluid-mediated processes influence local temperatures, stress, and mechanical properties leading to slip (de)localization along faults (Brantut & Platt, 2017; Hirono et al., 2013). Secondary mineral textures on slip surfaces track mechanochemical transformations that promote earthquake rupture propagation or energy dissipation via plastic deformation or creation of off-fault damage. Hematite, a common mineral associated with faults, exhibits textures that reflect the conditions of mineralization, related deformation rates, and micro- to nanoscale deformation mechanisms (e.g., McDermott et al., 2017, 2021; Moser et al., 2017). Hematite (U-Th)/He (hematite He) thermochronometry, when combined with textural observations, constrains the temperatures, rates, timing, and, importantly, depths of fault slip (Ault, 2020).

We investigate an exhumed >10 m^2 mirror-like, silica-rich bedrock fault surface of the seismogenic Hurricane fault zone, UT (Figure 1a). This fault extends >1 km along strike and locally preserves raised, light-reflective, and striated hematite patches, which we target for scanning and transmission electron microscopy (SEM, TEM) and texture-targeted hematite He thermochronometry. We document textures that reflect the role of comminution, fluids, and heat during seismic slip. Hematite He thermochronometry pinpoints the timing and brackets the depth at which these textures form. Our results indicate this fault surface developed in the shallow (~300 m depth) crust likely during the updip propagation of earthquake ruptures.

2. Hurricane Fault

The Hurricane fault is a N–S trending, 250 km-long, west-dipping normal fault; delineates the eastern boundary of the transition zone between the Colorado Plateau and Basin and Range tectonic provinces; and is part of the southern Intermountain Seismic Belt (Figure 1a; Arabasz & Julander, 1986; Smith et al., 1991). The Hurricane fault has six segments with independent rupture histories (Biek et al., 2010; Lund et al., 2007; Stewart & Taylor, 1996). The fault displaces Paleozoic and Mesozoic rocks, and Quaternary basalt flows, with net slip estimates of ~600–2,250 m (Biek, 2003; Lund et al., 2007; Stewart & Taylor, 1996). Slip on the Hurricane fault occurred since the late Miocene, concurrent with Basin and Range extension (Stewart & Taylor, 1996). Offset Quaternary basalt flows yield average slip rates of 0.21–0.57 mm/yr (Anderson & Mehnert, 1976; Lund et al., 2007). The fault accommodated at least 20 earthquakes >M 4 over the past century (Christenson & Nava, 1992), including the 1992 M 5.8 earthquake near St. George, UT (Stenner & Pearthree, 1999).

3. Hematite (U-Th)/He Thermochronometry From Fault Rocks

Hematite is common in the shallow portions of fault zones. It incorporates trace amounts of radiogenic U and Th and negligible ^{4}He during mineralization, making it amenable to (U-Th)/He thermochronometry (Farley & Flowers, 2012; Strutt, 1909; Wernicke & Lippolt, 1993). Individual hematite grains are the diffusion domain and polycrystalline aggregates, typical of fault rocks, exhibit poly-domain He diffusion behavior (Evenson et al., 2014; Farley, 2018; Farley & Flowers, 2012; Jensen et al., 2018). The hematite He closure temperature (T_c) increases with domain (grain) size from ~30 to 230°C (applying a 10°C/Ma cooling rate to ~1 nm-1 mm-thick plates; Farley, 2018).

Hematite He dates from fault rocks record various fault-related processes (Ault, 2020). These dates must be interpreted in the context of hematite morphology, deformation textures, grain-size distribution and thus T_c range, and post-formation thermal history. Depending on the ambient temperature conditions at which hematite forms or is deformed relative to the T_c, hematite may record mineralization (McDermott et al., 2021; Moser et al., 2017; Wu et al., 2019), cooling due to exhumation (Calzolari et al., 2018), or He loss associated with frictional heating and/or hydrothermal fluids (Ault et al., 2016; McDermott et al., 2017). Comminution or recrystallization during slip can modify the T_c, making an aliquot susceptible to He loss at lower temperatures (Ault et al., 2015).

4. Samples and Methods

Hematite samples are from a ~10 m^2 bedrock fault with a smooth, light-reflective surface that cuts the Rock Canyon Member of the Triassic Moenkopi Formation (Fm) (37°13′ 23.44″ N, 113°15′ 29.88″ W; Figures 1b–1e). The fault strikes ~170°S with a near-vertical W dip and has dip-slip slickenlines, visible on the hematite patches. Semicontinuous mirrored exposures extend along-strike for ~1.1 km in the Anderson junction segment (Figures 1b and 1d). We extracted three samples (HUR1/HUR2, HUR3, HUR4; Figure 1e) from separate hematite patches on the fault surface, and examined five plan view and 36 cross-sectional aliquots from them with a field emission-SEM. Back-scattered and secondary electron images characterize hematite nano- and microstructures, grain morphologies, and grain sizes. Sample HUR4 was dissected with a focused ion beam-SEM to produce a cross-sectional lamella for scanning/transmission electron microscopy (S/TEM). S/TEM analyses included bright-field, dark-field, and TEM imaging, nanoscale energy dispersive X-ray spectroscopy (EDS), and diffraction analysis. U, Th, and He contents of hematite aliquots from each sample were measured in two sessions. Sample preparation and all analytical methods (Text S1–S4), as well as SEM (Figures S1–S10) and S/TEM (Figures S11–S14) image catalogs, are detailed in the Supporting Information S1.

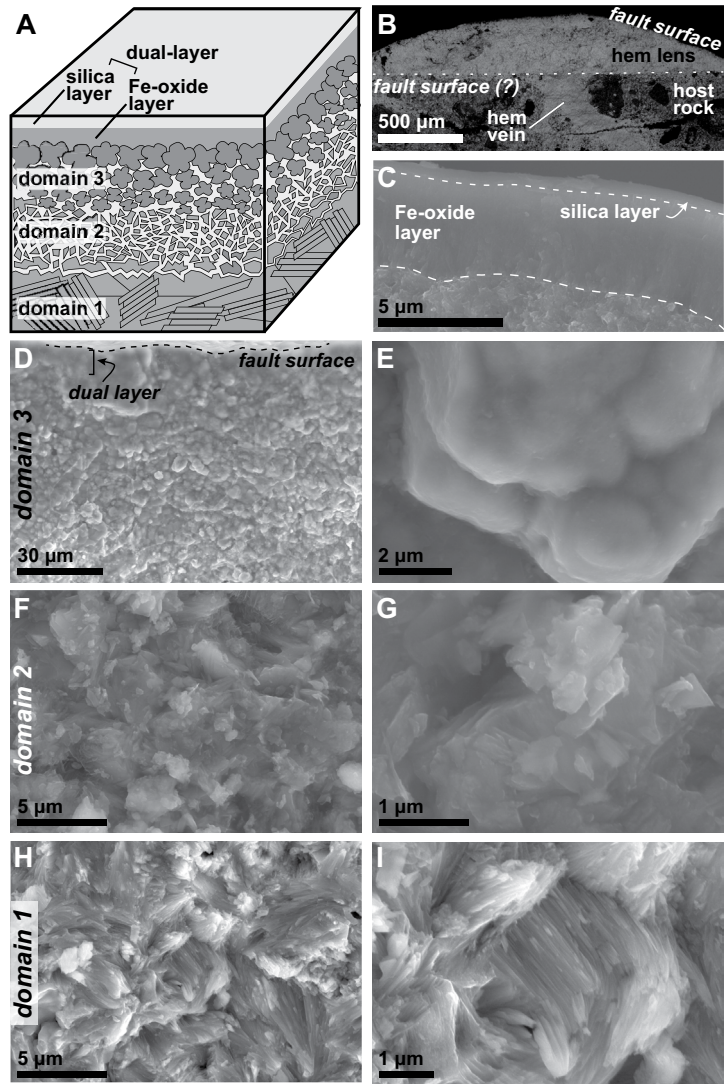

Figure 2. (a) Schematic block diagram of hematite patch showing textural domains and dual-layer. (b–i) Scanning electron microscopy secondary electron images of sample HUR3 in cross-section (b), dual surface layer (c), and domains 3 (d and e), 2 (f and g), and 1 (h and i).

5. Results

5.1. Hematite Textures

Hematite occurs as elongate, <cm-scale, striated patches, raised 500 µm-1 mm above the surrounding slip surface (Figure 1e). Patches are spatially associated with mm-thick hematite veins oriented oblique to the slip surface (Figures 1e and 2). These patches overlie a host rock micro-breccia (~5 cm-thick) with mm- to µm-diameter, angular chert and lesser limestone clasts (Figure 1e). Patches exhibit three textural domains broadly perpendicular to the slip surface and an outer <3 µm-thick "dual-layer" with distinct textural and compositional properties (Figures 2a and S7). Domain 1 hematite, observed >130 µm away from the surface, comprises randomly oriented, high-aspect-ratio plates that are ~40–150 nm-thick (Figures 2h and 2i; Table S1). Void spaces are preserved between clusters of densely stacked plates (Figures S1 and S8a–S8d). Domain 2, >60 µm from the surface, is characterized by dominantly subangular hematite fragments and broken plates that are ~60–640 nm-thick (Figures 2f and 2g; Table S1).

Domain 3 occurs <60 µm from the slip surface (Figures 2d and 2e). Here, bulbous hematite aggregates have smooth, internally featureless lobes (~140 nm–4 µm in diameter), which lack well-defined boundaries at

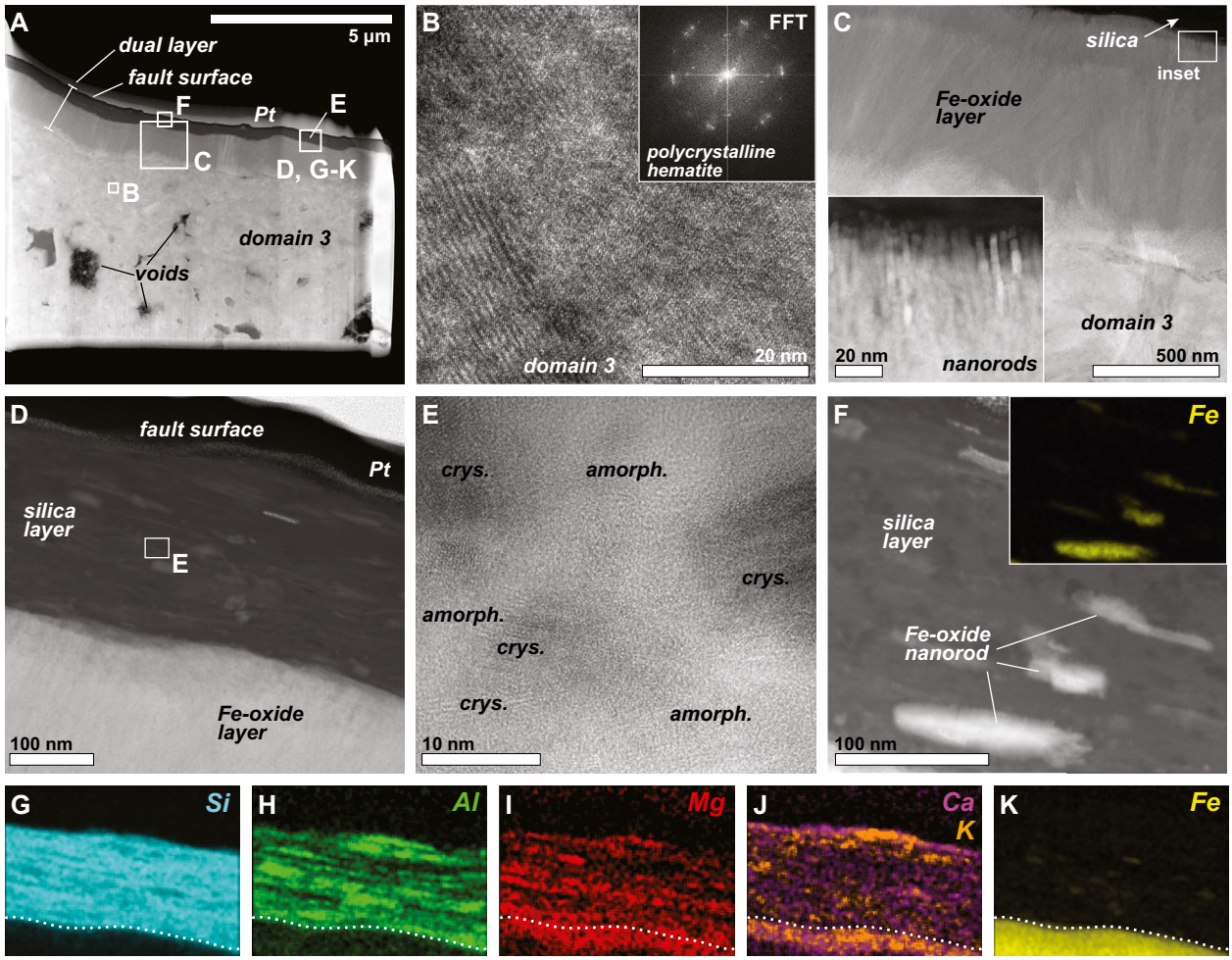

Figure 3. (a) Scanning/transmission electron microscopy (S/TEM) dark field image of HUR4 lamella; locations of (b–k) denoted. (b) High-resolution (HR) TEM and Fast Fourier Transform (FFT) images of domain 3. (c) S/TEM dark field images of basal Fe-oxide layer. (d) S/TEM bright field image and (e) HRTEM of upper silica layer; amorph. = amorphous, crys. = crystalline (f) Fe-oxide nanorods in silica layer in S/TEM bright field; inset: associated S/TEM EDS Fe map. (g–k) Co-located S/TEM EDS chemical maps of Si (g), Al (h), Mg (i), Ca and K (j), and Fe (k); white dashed line marks Fe-oxide-silica boundary.

the SEM-scale (Table S1). TEM, including fast Fourier transform patterns, revealed that some lobes comprise crystalline, radially oriented, high-aspect-ratio platelets that are ~10 nm-wide and have six-fold coordination consistent with hematite (Figures 3a and 3b). S/TEM EDS detected diffuse Si, local Al, and isolated, nm-scale zones enriched in Ti within this hematite (Figure S14). Local voids <5 µm from the surface contain crystalline Si phases and amorphous Mg-oxide (Figures 3a and S14). The presence, thickness, and development of hematite textural domains vary parallel and perpendicular to the slip surface and between patches.

5.2. Fault Surface Dual Layer

The hematite slip surfaces exhibit a ~0.5–3 µm-thick surface layer that appears smooth and featureless at the SEM scale (Figure 2c). TEM imaging shows this layer has two components ("dual" layer; Figures 3a and 3c–3f). The basal layer is defined by elongate, densely packed Fe-oxide rods that are <4 nm in diameter with their long axis perpendicular to the slip surface (Figure 3c). Fe-oxide nanorods contain Mg, Ca, and K at the contact with an overlying ~200 nm-thick silica layer (Figures 3g–3j). High-resolution TEM (Figure 3e) and diffraction patterns indicate the silica is amorphous. This silica has higher Al content than the basal Fe-oxide, contains Mg, and the uppermost portion is enriched in K and Ca (Figures 3h and 3j). It contains isolated Fe-oxide nanorods oriented with their long axis parallel to the fault surface (Figure 3f). The nature

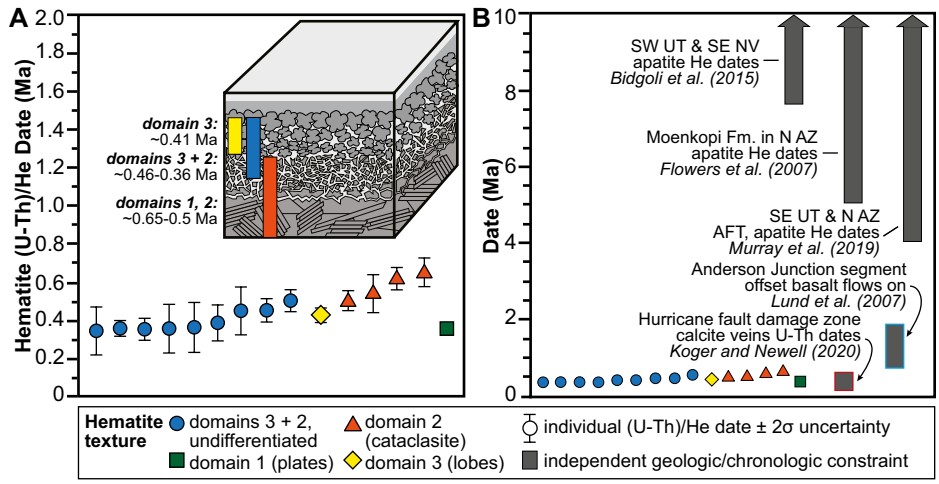

Figure 4. (a) Individual hematite (U-Th)/He dates with 2σ analytical uncertainties classified by texture. Inset: hematite block diagram with interpreted relationships between domains and dates. (b) Comparison of hematite He dates with local fault-related geochronology (Koger & Newell, 2020; Lund et al., 2007) and regional thermochronometry (Bidgoli et al., 2015; Flowers et al., 2007; Murray et al., 2019).

of the contact between the dual-layer and underlying hematite varies along the slip surface and between different hematite patches. For example, the contact is sharp in HUR3 where domain 2 underlies the dual layer and domain 3 is locally absent (e.g., Figure 2c) and is gradational above domain 3 within HUR4 (Figure 3c).

5.3. Hematite (U-Th)/He Data

We initially acquired 14 hematite He dates from sample HUR1/HUR2. Aliquots were not examined via SEM before (U-Th)/He analyses, but stereoscopic inspection and SEM-imaging of representative aliquots indicated dated material is dominantly domain 3 and some domain 2. Nine hematite He dates from this sample yield a mean of 0.39 ± 0.04 Ma (±1σ standard deviation; Figure 4a; Table S2). Individual dates range from 0.46 ± 0.04 Ma to 0.36 ± 0.10 Ma (date ± 2σ analytical uncertainty) with Th/U of 0.22–0.37. We report (Table S2) but do not consider further an additional five analyses because of likely U volatilization during degassing and possible secular disequilibrium (Text S4; Figure S15).

We subsequently used SEM to pre-screen aliquots prior to (U-Th)/He analysis to target each textural domain (cf. McDermott et al., 2017). Analyzed aliquots were small to ensure textural and mineralogical homogeneity, resulting in U and Th yields for some aliquots near the analytical resolution limit. A subset of aliquots experienced U volatilization during laser heating and some dates sit on the cusp of secular equilibrium for the (U-Th)/He system (see discussion in Text S4; Table S2). All pre-screened hematite He dates ($n = 15$) are reported in Table S2 and here we discuss six robust individual hematite He dates from samples HUR1/HUR2 and HUR 3 (Figure 4a). An individual date from domain 1 in HUR1/HUR2 is 0.36 ± 0.02 Ma. Dates from domain 2 in HUR3 are 0.65 ± 0.06 Ma, 0.61 ± 0.05 Ma, 0.53 ± 0.08 Ma, and 0.50 ± 0.04 Ma, with a mean of 0.57 ± 0.07 Ma. The date from domain 3 in HUR3 is 0.41 ± 0.03 Ma. These aliquots have Th/U of 0.16–0.35.

6. Discussion

6.1. Textural Relationships and Interpretations

Hematite morphology and textural relationships inform the mechanical, fluid, and thermally mediated processes operative during Hurricane fault slip. The spatial association between hematite patches and veins indicates a genetic relationship (Figure 2b). Domain 1 textures are consistent with shallow hydrothermal hematite precipitation (Figures 2h and 2i; cf. Ault et al., 2016). Angular hematite fragments in domain 2 are generated by cataclasis of domain 1 material during slip. Discrete surfaces at the top and base of the hematite patches support, but do not require, at least two slip events (Figure 2b). Veins and patches cut and

overlie the host rock microbreccia indicating the fault surface was repeatedly reactivated with progressively localized deformation.

Domain 3 hematite textures and the dual surface layer comprise material that has been fully transformed by fault slip. Domain 3 hematite and the basal Fe-oxide layer are sourced from hematite in domains 1 and 2. The bulbous domain 3 lobes grade into Fe-oxide nanorods that grew toward the slip surface (Figures 3a and 3c). The overlying amorphous silica with trace Al, Mg, Ca, and K (Figures 3e–3k) is likely sourced from the adjacent Rock Canyon Member underlying the patches and/or material on the opposing side of the fault. The Rock Canyon Member conglomerate contains chert and limestone clasts, and carbonate cement and veins. The preservation of amorphous silica at the slip surface and complete transformation of domain 3 hematite suggest this material was collectively amorphous. Al present within the amorphous silica implies it was hydrous (Figure 3h; Faber et al., 2014; Oehler, 1976). Individual nanorods suspended in the amorphous, hydrous silica (Figure 3f) originated from the underlying Fe-oxide layer, implying that solidification of amorphous silica occurred syn- to post-crystallization of Fe-oxide nanorods. Portions of the larger outcrop surface are mirror-like, suggesting extensive amorphous silica on the fault surface (Figures 1c and 1d).

We suggest the development of domains 2 and 3 textures, and the dual layer, involves (a) coseismic comminution of pre-existing hematite and conglomerate, (b) mechanical, fluid, and temperature assisted amorphization, and (c) rapid growth of sintered lobes and nanorods, and silica solidification in the syn- to post-seismic period. An increase in particle surface area during cataclasis promotes amorphization (Aretusini et al., 2017; Kaneki et al., 2020). Domain 2 provides a vestige of the comminution that facilitated this process. Amorphization may also be associated with fluid-mediated chemical reactions (Hirono et al., 2013) and frictional heating (Brantut et al., 2008; Hayward et al., 2016), but it does not require high temperatures (Pec et al., 2012; Yund et al., 1990).

Differences in textures between Hurricane fault hematite patches and previously documented hematite "fault mirrors" imply disparate temperatures and conditions during coseismic slip. Mirrors can exhibit triple-junction-forming (polygonal) grains that lack shape and crystallographic preferred orientation within ~50 μm of the slip surface (Ault et al., 2015, 2019; McDermott et al., 2017), analogous to textures observed in high-temperature experiments ($T > 800$°C; Siemes et al., 2003, 2011; Vallina et al., 2014). Locally mirrored zones comprising sintered nanoparticles created during high-velocity hematite deformation experiments yield >70% He loss during slip, consistent with transient temperature rise >800°C (Calzolari et al., 2020). We lack direct constraints on Hurricane fault slip temperatures but suggest they must be markedly lower than those achieved on hematite fault mirrors. Hydrothermal synthesis produces similarly sized hematite nanorods in minutes to hours at temperatures ~100–200°C (Almeida et al., 2010; Tadic et al., 2019; Wheeler et al., 2012). As discussed below, our samples are at ~300 m depth during slip, where normal stresses are low (~6.5 MPa) and interstitial fluids are prevalent (Gleeson et al., 2016). Prior work supports the presence of shallow hydrothermal fluids in the Hurricane fault zone between ~540 and 90 ka, overlapping our hematite He dates (Koger & Newell, 2020). Additionally, pore fluid vapourization during coseismic slip may enhance fluid pressurization, dampen temperature rise, and promote earthquake rupture propagation on thin slip surfaces like the Hurricane fault (Chen et al., 2017).

6.2. Timing and Depth of Fault Slip From Hematite (U-Th)/He Thermochronometry

Individual hematite He dates are ~0.65–0.36 Ma. To interpret these results, we first compare hematite He dates and grain-size dependent T_c estimates with geologic and chronometric constraints on the ambient thermal history (cf. McDermott et al., 2021). We calculate T_c estimates from our oldest dates (domain 2) using the range of particle half-widths, diffusion kinetics of Farley (2018), and a 10°C/Ma cooling rate. Average half-widths are 60–640 nm, corresponding to T_c of ~65–100°C, which broadly overlaps with data from the other domains (Table S3). This T_c range is similar to the apatite (U-Th)/He (apatite He) T_c, which is ~30–90°C (Flowers et al., 2009). There are no reported conventional low-temperature thermochronometry data from the Moenkopi Fm in the Hurricane fault footwall or from any units in the vicinity of our study area. However, apatite He and apatite fission track dates from across southern UT and northern AZ are all >4 Ma (Figure 4b; Bidgoli et al., 2015; Flowers et al., 2007; Murray et al., 2019). The most proximal apatite He dates from the Moenkopi Fm (~120 km from our study area) are ~5–77 Ma and radiation damage-He diffusivity

data patterns reflect limited burial (heating) followed by late Miocene cooling (Flowers et al., 2007). If our hematite formed at depth and hematite He dates track cooling due to regional erosion, then we would expect the hematite and apatite He dates to overlap, but they do not.

Offset Quaternary basalt flows along the Anderson Junction segment and Virgin River incision constrain the local erosion and footwall exhumation history. The closest basalt flow erupted 0.35 ± 0.05 Ma (date ± 2σ uncertainty; Sanchez, 1995) and is vertically offset across the Hurricane fault by 73 m. Older flows along this segment indicate ~440 m of fault offset in the last ~1.5 Ma (Lund et al., 2007). The calculated incision rate for the nearby Virgin River in the Hurricane fault footwall is 338 m/Ma (Walk et al., 2019), consistent with ~220 m of incision since our oldest ~0.65 Ma hematite He date. Fault offset and incision estimates indicate <300 m of total exhumation over the past ~0.65 Ma, far lower than the required ~2 km mineralization depth if our hematite He dates reflected ambient cooling (using calculated T_c, 30°C/km geothermal gradient, 15°C mean surface temperature). These comparisons indicate that hematite He dates must record mineralization and/or some other faulting-specific process at ~300 m depth.

Results from microtexturally pre-screened aliquots allow us to refine our hematite He data interpretations (Figure 4a). Hematite precipitated as plates preserved in domain 1, but the sole robust single-aliquot hematite He date from this domain is younger than domain 2 dates (Figure 4a). Domain 1 contains void spaces that exceed the He stopping distance (~14–16 μm), likely causing excess He loss and the anomalously young date (Huber et al., 2019; Huff et al., 2020). Domain 2 cataclastic hematite likely retained its He budget since formation because deformation experiments show that comminution during seismic slip does not induce substantial He loss (Calzolari et al., 2020). The ~0.65–0.5 Ma domain 2 dates record the time of initial hematite precipitation in the coseismic or immediate post-seismic period (Nuriel et al., 2019; Williams et al., 2017).

Comminution, amorphization, and regrowth of new hematite (domain 3) occurred during a subsequent seismic slip event at ~0.46–0.36 Ma. The sole domain 3 hematite He date (~0.41 Ma) falls within the range of dates from HUR1/HUR2 aliquots (~0.46–0.36 Ma) comprising dominantly domain 3 material (Figure 4a). Amorphization and transformation of domain 3 hematite yields complete He loss at that time. This requires that any thermal perturbation associated with fault slip is both highly localized at the slip surface and of low enough magnitude to not induce He loss in domains 2 and 1 hematite.

7. Implications for Shallow Earthquake Rupture Propagation

Our data capture episodes of seismic slip along the Anderson Junction segment of the Hurricane fault, broadly coeval with documented shallow earthquake-related deformation elsewhere along the fault (Figure 4b; Koger & Newell, 2020). Hematite He data patterns and erosion estimates require that hematite mineralization and seismic slip occurred at ~300 m depth. Thus, observed textures reflect the up-dip propagation of earthquake ruptures from the seismogenic zone. Although we cannot rule out distributed deformation along other sub-parallel fault strands (Figure 1b) or the creation of off-fault damage during other earthquakes, some Pleistocene earthquakes were preferentially localized on this discrete fault surface. Paleoseismic investigations indicate segments of the Hurricane fault experienced multiple large magnitude earthquakes (M 6.4–7.3; Lund et al., 2007). Given the >1 km extent of this fault along strike (Figure 1b), it was likely repeatedly reactivated as ruptures propagated toward the surface from depth.

The Hurricane fault exposure detailed in this study provides a rare window into how the uppermost crust accommodates earthquake energy. Our data reveal that at ~300 m depth, comminution and hydrothermal processes work constructively to transform fault materials even at the nanoscale to promote slip localization and rupture propagation (cf. Hirono et al., 2013). The shallowest parts of some bedrock fault systems do not necessarily exhibit voluminous fault damage, but rather large m- to km-scale discrete slip surfaces that repeatedly distribute earthquake energy. Thus, the shallow crust hosts a diversity of structures and evolving mechanical properties that promote or inhibit rupture propagation. Integration of textural and thermochronometric data from shallowly exhumed faults with complementary data from deformation experiments can provide direct observables such as fault zone width, coefficient of friction and constitutive behavior of fault materials, and spatial heterogeneities in these properties, which underpin geophysical models of fault slip and strong ground motion.

Data Availability Statement

Data contained within the Supporting Information S1 is archived and freely available at https://doi.org/10.6084/m9.figshare.15175476, and hematite He analyses are available at Geochron.org (http://www.geochron.org/results.php?pkey=34293).

Acknowledgments
The authors thank Fen-Ann Shen (USU), Brian Van Devener and Randy Polson (Utah), Peter Reiners and Uttam Chowdhury (UA) for analytical assistance; and Marissa Tremblay and David Malone for thoughtful reviews. Research was supported by NSF CAREER grant EAR-1654628 (Ault) and USU Peak Summer Fellowship, UROP, and COS Minigrant (Taylor). M. L. Odlum was supported by NSF EAR-1952905.

References

Almeida, T. P., Fay, M. W., Zhu, Y., & Brown, P. D. (2010). Hydrothermal growth mechanism of α-Fe 2 O 3 nanorods derived by near in situ analysis. *Nanoscale*, *2*, 2390–2399. https://doi.org/10.1039/c0nr00280a

Anderson, R. E., & Mehnert, H. H. (1976). *Reinterpretation of the history of the Hurricane fault in Utah*. Denver, CO: Rocky Mountain Associated of Geologists and Utah Geological Association.

Arabasz, W. J., & Julander, D. R. (1986). Geometry of seismically active faults and crustal deformation within the Basin and Range-Colorado Plateau transition in Utah. *Geological Society of America Special Paper*, *208*, 43–74. https://doi.org/10.1130/spe208-p43

Aretusini, S., Mittempergher, S., Plümper, O., Spagnuolo, E., Gualtieri, A., & Di Toro, G. (2017). Production of nanoparticles during experimental deformation of smectite and implications for seismic slip. *Earth and Planetary Science Letters*, *463*, 221–231. https://doi.org/10.1016/j.epsl.2017.01.048

Ault, A. K. (2020). Hematite fault rock thermochronometry and textures inform fault zone processes. *Journal of Structural Geology*, *133*(104002), 10. https://doi.org/10.1016/j.jsg.2020.104002

Ault, A. K., Frenzel, M., Reiners, P. W., Woodcock, N. H., & Thomson, S. N. (2016). Record of paleofluid circulation in faults revealed by hematite (U-Th)/He and apatite fission-track dating: An example from Gower Peninsula fault fissures, Wales. *Lithosphere*, *8*, 379–385. https://doi.org/10.1130/l522.1

Ault, A. K., Jensen, J. L., McDermott, R. G., Shen, F.-A., & Van Devener, B. R. (2019). Nanoscale evidence for temperature-induced transient rheology and postseismic fault healing. *Geology*, *47*, 1203–1207. https://doi.org/10.1130/g46317.1

Ault, A. K., Reiners, P. W., Evans, J. P., & Thomson, S. N. (2015). Linking hematite (U-Th)/He dating with the microtextural record of seismicity in the Wasatch fault damage zone, Utah, USA. *Geology*, *43*, 771–774. https://doi.org/10.1130/g36897.1

Barbot, S., Fialko, Y., & Sandwell, D. (2008). Effect of a compliant fault zone on the inferred earthquake slip distribution. *Journal of Geophysical Research*, *113*, B06404. https://doi.org/10.1029/2007jb005256

Bidgoli, T. S., Stockli, D. F., & Walker, J. D. (2015). Low-temperature thermochronologic constraints on the kinematic histories of the Castle Cliffs, Tule Springs, and Mormon Peak detachments, southwestern Utah and southeastern Nevada. *Geosphere*, *11*, 850–867. https://doi.org/10.1130/ges01083.1

Biek, R. (2003). Geologic Map of the Hurricane Quadrangle, Washington County, Utah, Utah Geological Survey Map, 187 ed. Utah Geological Survey, Salt Lake City, UT.

Biek, R., Rowley, P., Hayden, J., Hacker, D., Willis, G., Hintze, L., et al. (2010). *Geologic map of the St. George and east part of the Clover Mountains, 30' x 60' quadrangles, Washington and Iron counties, Utah*. Salt Lake City, UT: Utah Geological Survey.

Brantut, N., & Platt, J. D. (2017). Dynamic weakening and the depth dependence of earthquake faulting. *Fault zone dynamic processes: Evolution of fault properties during seismic rupture, Geophysical Monograph Series*, *227*, 171–194. https://doi.org/10.1002/9781119156895.ch9

Brantut, N., Schubnel, A., Rouzaud, J. N., Brunet, F., & Shimamoto, T. (2008). High-velocity frictional properties of a clay-bearing fault gouge and implications for earthquake mechanics. *Journal of Geophysical Research*. *113*. https://doi.org/10.1029/2007jb005551

Calzolari, G., Ault, A. K., Hirth, G., & McDermott, R. G. (2020). Hematite (U-Th)/He thermochronometry detects asperity flash heating during laboratory earthquakes. *Geology*, *48*, 514–518. https://doi.org/10.1130/g46965.1

Calzolari, G., Rossetti, F., Ault, A. K., Lucci, F., Olivetti, V., & Nozaem, R. (2018). Hematite (U-Th)/He thermochronometry constrains strike-slip faulting on the Kuh-e-Faghan fault, central Iran. *Tectonophysics*, *728–729*, 41–54. https://doi.org/10.1016/j.tecto.2018.01.023

Chen, J., Niemeijer, A., Yao, L., & Ma, S. (2017). Water vaporization promotes coseismic fluid pressurization and buffers temperature rise. *Geophysical Research Letters*, *44*, 2177–2185. https://doi.org/10.1002/2016gl071932

Christenson, G. E., Nava, S. J. (1992), *Earthquake hazards of southwestern Utah*.

Dolan, J. F., & Haravitch, B. D. (2014). How well do surface slip measurements track slip at depth in large strike-slip earthquakes? The importance of fault structural maturity in controlling on-fault slip versus off-fault surface deformation. *Earth and Planetary Science Letters*, *388*, 38–47. https://doi.org/10.1016/j.epsl.2013.11.043

Evenson, N. S., Reiners, P. W., Spencer, J., & Shuster, D. L. (2014). Hematite and Mn oxide (U-Th)/He dates from the Buckskin-Rawhide detachment system, western Arizona: Constraining the timing of mineralization and hematite (U-Th)/He systematics. *American Journal of Science*, *314*, 1373–1435. https://doi.org/10.2475/10.2014.01

Faber, C., Rowe, C. D., Miller, J. A., Fagereng, A., & Neethling, J. H. (2014). Silica gel in a fault slip surface: Field evidence for palaeo-earthquakes? *Journal of Structural Geology*, *69*, 108–121. https://doi.org/10.1016/j.jsg.2014.09.021

Fagereng, Å., & Toy, V. G. (2011). Geology of the earthquake source: An introduction. *Geological Society, London, Special Publications*, *359*, 1–16. https://doi.org/10.1144/sp359.1

Farley, K. A. (2018). Helium diffusion parameters of hematite from a single-diffusion-domain crystal. *Geochimica et Cosmochimica Acta*, *231*, 117–129. https://doi.org/10.1016/j.gca.2018.04.005

Farley, K. A., & Flowers, R. M. (2012). (U-Th)/Ne and multidomain (U-Th)/He systematics of a hydrothermal hematite from eastern Grand Canyon. *Earth and Planetary Science Letters*, *359–360*, 131–140. https://doi.org/10.1016/j.epsl.2012.10.010

Field, E., Biasi, G., Bird, P., Dawson, T., Felzer, K., Jackson, D., et al. (2013). The uniform California earthquake rupture forecast, version 3 (UCERF3)—The time-independent model (US Geological Survey Open-File Report 2013–1165, California Geological Survey Special Report 228, and Southern California Earthquake Center Publication 1792, US Geological Survey, 2013). *California Geological Survey Special Report 228, and Southern California Earthquake Center Publication*, *1792*, 97.

Flowers, R. M., Ketcham, R. A., Shuster, D. L., & Farley, K. A. (2009). Apatite (U-Th)/He thermochronometry using a radiation damage accumulation and annealing model. *Geochimica et Cosmochimica Acta*, *73*, 2347–2365. https://doi.org/10.1016/j.gca.2009.01.015

Flowers, R. M., Shuster, D. L., Wernicke, B. P., & Farley, K. A. (2007). Radiation damage control on apatite (U-Th)/He dates from the Grand Canyon region, Colorado Plateau. *Geology*, *35*, 447–450. https://doi.org/10.1130/g23471a.1

Gleeson, T., Befus, K. M., Jasechko, S., Luijendijk, E., & Cardenas, M. B. (2016). The global volume and distribution of modern groundwater. *Nature Geoscience*, *9*, 161–167. https://doi.org/10.1038/ngeo2590

Hayward, K. S., Cox, S. F., Gerald, J. D. F., Slagmolen, B. J., Shaddock, D. A., Forsyth, P. W., et al. (2016). Mechanical amorphization, flash heating, and frictional melting: Dramatic changes to fault surfaces during the first millisecond of earthquake slip. *Geology*, *44*, 1043–1046. https://doi.org/10.1130/g38242.1

Hirono, T., Tanikawa, W., Honda, G., Kameda, J., Fukuda, J.-i., & Ishikawa, T. (2013). Importance of mechanochemical effects on fault slip behavior during earthquakes. *Geophysical Research Letters*, *40*, 2988–2992. https://doi.org/10.1002/grl.50609

Huber, C., Guenthner, W. R., & Karani, H. (2019). A new correction for He loss applied to (U-Th)/He Dating of grains with complex shapes and polymineralic aggregates. *Geochemistry, Geophysics, Geosystems*.

Huff, D. E., Holley, E., Guenthner, W. R., & Kaempfer, J. M. (2020). Fe-oxides in jasperoids from two gold districts in Nevada: Characterization, geochemistry, and (U-Th)/He dating. *Geochimica et Cosmochimica Acta*, *286*, 72–102. https://doi.org/10.1016/j.gca.2020.07.014

Jensen, J. L., Siddoway, C. S., Reiners, P. W., Ault, A. K., Thomson, S. N., & Steele-MacInnis, M. (2018). Single-crystal hematite (U-Th)/He dates and fluid inclusions document Cryogenian seismic clastic injection in granite. *Earth and Planetary Science Letters*, *500*, 145–155. https://doi.org/10.1016/j.epsl.2018.08.021

Kaneki, S., Oohashi, K., Hirono, T., & Noda, H. (2020). Mechanical amorphization of synthetic fault gouges during rotary-shear friction experiments at subseismic to seismic slip velocities. *Journal of Geophysical Research: Solid Earth*, *125*, e2020JB019956. https://doi.org/10.1029/2020jb019956

Kaneko, Y., & Fialko, Y. (2011). Shallow slip deficit due to large strike-slip earthquakes in dynamic rupture simulations with elasto-plastic off-fault response. *Geophysical Journal International*, *186*, 1389–1403. https://doi.org/10.1111/j.1365-246x.2011.05117.x

Klinger, Y., Okubo, K., Vallage, A., Champenois, J., Delorme, A., Rougier, E., et al. (2018). Earthquake damage patterns resolve complex rupture processes. *Geophysical Research Letters*, *45*, 10279–10287. https://doi.org/10.1029/2018gl078842

Koger, J. M., & Newell, D. L. (2020). Spatiotemporal history of fault–fluid interaction in the Hurricane fault, western USA. *Solid Earth*, *11*, 1969–1985. https://doi.org/10.5194/se-11-1969-2020

Lund, W. R., Hozik, M., & Hatfield, S. (2007). *Paleoseismic investigation and long-term slip history of the Hurricane Fault in southwestern Utah*. Salt Lake City, UT: Utah Geological Survey.

McDermott, R. G., Ault, A. K., & Caine, J. S. (2021). Dating fault damage along the eastern Denali fault zone with hematite (U-Th)/He thermochronometry. *Earth and Planetary Science Letters*, *563*, 116872. https://doi.org/10.1016/j.epsl.2021.116872

McDermott, R. G., Ault, A. K., Evans, J. P., & Reiners, P. W. (2017). Thermochronometric and textural evidence for seismicity via asperity flash heating on exhumed hematite fault mirrorsWasatch fault zone, UT, USA. *Earth and Planetary Science Letters*, *471*, 85–93. https://doi.org/10.1016/j.epsl.2017.04.020

Moser, A. C., Evans, J. P., Ault, A. K., Janecke, S. U., & Bradbury, K. K. (2017). (U-Th)/He thermochronometry reveals Pleistocene punctuated deformation and synkinematic hematite mineralization in the Mecca Hills, southernmost San Andreas Fault zone. *Earth and Planetary Science Letters*, *476*, 87–99. https://doi.org/10.1016/j.epsl.2017.07.039

Murray, K. E., Reiners, P. W., Thomson, S. N., Robert, X., & Whipple, K. X. (2019). The thermochronologic record of erosion and magmatism in the Canyonlands region of the Colorado Plateau. *American Journal of Science*, *319*, 339–380. https://doi.org/10.2475/05.2019.01

Nevitt, J. M., Brooks, B. A., Catchings, R. D., Goldman, M. R., Ericksen, T. L., & Glennie, C. L. (2020). Mechanics of near-field deformation during co-and post-seismic shallow fault slip. *Scientific Reports*, *10*, 1–13. https://doi.org/10.1038/s41598-020-61400-9

Nuriel, P., Miller, D. M., Schmidt, K. M., Coble, M. A., & Maher, K. (2019). Ten-million years of activity within the Eastern California Shear Zone from U–Pb dating of fault-zone opal. *Earth and Planetary Science Letters*, *521*, 37–45. https://doi.org/10.1016/j.epsl.2019.05.047

Oehler, J. H. (1976). Hydrothermal crystallization of silica gel. *Geological Society of America Bulletin*, *87*, 1143–1152. https://doi.org/10.1130/0016-7606(1976)87<1143:HCOSG>2.0.CO;2

Pec, M., Stünitz, H., Heilbronner, R., Drury, M., & de Capitani, C. (2012). Origin of pseudotachylites in slow creep experiments. *Earth and Planetary Science Letters*, *355*, 299–310. https://doi.org/10.1016/j.epsl.2012.09.004

Petersen, M. D., Moschetti, M. P., Powers, P. M., Mueller, C. S., Haller, K. M., Frankel, A. D., et al. (2015). The 2014 United States national seismic hazard model. *Earthquake Spectra*, *31*, S1–S30. https://doi.org/10.1193/120814eqs210m

Rockwell, T. K., & Ben-Zion, Y. (2007). High localization of primary slip zones in large earthquakes from paleoseismic trenches: Observations and implications for earthquake physics. *Journal of Geophysical Research*, *112*. https://doi.org/10.1029/2006jb004764

Roten, D., Olsen, K., & Day, S. (2017). Off-fault deformations and shallow slip deficit from dynamic rupture simulations with fault zone plasticity. *Geophysical Research Letters*, *44*, 7733–7742. https://doi.org/10.1002/2017gl074323

Sanchez, A. (1995). *Mafic volcanism in the Colorado plateau/basin-and-range transition zone, Hurricane, Utah*.

Scholz, C. H. (2002). *The Mechanics of Earthquakes and Faulting*. Cambridge, United Kingdom: Cambridge University Press.

Sibson, R. H. (1983). Continental fault structure and the shallow earthquake source. *Journal of the Geological Society*, *140*, 741–767. https://doi.org/10.1144/gsjgs.140.5.0741

Siemes, H., Klingenberg, B., Rybacki, E., Naumann, M., Schafer, W., Jansen, E., & Rosiere, C. A. (2003). Texture, microstructure, and strength of hematite ores experimentally deformed in the temperature range 600-1100 ºC and at strain rates between 10^{-4} and 10^{-6} s^{-1}. *Journal of Structural Geology*, *25*, 1371–1391. https://doi.org/10.1016/s0191-8141(02)00184-0

Siemes, H., Rybacki, E., Klingenberg, B., & Rosière, C. A. (2011). Development of a recrystallized grain size piezometer for hematite based on high-temperature torsion experiments. *European Journal of Mineralogy*, *23*, 293–302. https://doi.org/10.1127/0935-1221/2011/0023-2103

Smith, R., Arabasz, W., Slemmons, D., Engdahl, E., Zoback, M., & Blackwell, D. (1991). Seismicity of the intermountain seismic belt. *Neotectonics of North America*, *1*, 185–228.

Stenner, H. D., & Pearthree, P. A. (1999). Paleoseismology of the Anderson Junction section of the Hurricane Fault, northwestern Arizona and southwestern Utah. Tucson, AZ: Arizona Geological Survey.

Stewart, M. E., & Taylor, W. J. (1996). Structural analysis and fault segment boundary identification along the Hurricane fault in southwestern Utah. *Journal of Structural Geology*, *18*, 1017–1029. https://doi.org/10.1016/0191-8141(96)00036-3

Strutt, R. J. (1909). The accumulation of helium in geological time, II. *Proceedings of the Royal Society of London A*, *83*, 96–99. https://doi.org/10.1098/rspa.1909.0081

Tadic, M., Trpkov, D., Kopanja, L., Vojnovic, S., & Panjan, M. (2019). Hydrothermal synthesis of hematite (α-Fe2O3) nanoparticle forms: Synthesis conditions, structure, particle shape analysis, cytotoxicity and magnetic properties. *Journal of Alloys and Compounds*, *792*, 599–609. https://doi.org/10.1016/j.jallcom.2019.03.414

Vallina, B., Rodriguez-Blanco, J. D., Brown, A. P., Benning, L. G., & Blanco, J. A. (2014). Enhanced magnetic coercivity of a-Fe_2O_3 obtained from carbonated 2-line ferrihydrite. *Journal of Nanoparticle Research*, *16*(2232), 10. https://doi.org/10.1007/s11051-014-2322-5

Walk, C. J., Karlstrom, K. E., Crow, R. S., & Heizler, M. T. (2019). Birth and evolution of the Virgin River fluvial system:~ 1 km of post–5 Ma uplift of the western Colorado Plateau. *Geosphere*, *15*, 759–782. https://doi.org/10.1130/ges02019.1

Wernicke, R. S., & Lippolt, H. J. (1993). Botryoidal hematite from the Schwarzwald (Germany): Heterogeneous uranium distributions and their bearing on the helium dating method. *Earth and Planetary Science Letters*, *114*, 287–300. https://doi.org/10.1016/0012-821x(93)90031-4

Wheeler, D. A., Wang, G., Ling, Y., Li, Y., & Zhang, J. Z. (2012). Nanostructured hematite: Synthesis, characterization, charge carrier dynamics, and photoelectrochemical properties. *Energy & Environmental Science*, *5*, 6682–6702. https://doi.org/10.1039/c2ee00001f

Williams, R. T., Goodwin, L. B., Sharp, W. D., & Mozley, P. S. (2017). Reading a 400,000-year record of earthquake frequency for an intraplate fault. *Proceedings of the National Academy of Sciences*, *114*, 4893–4898. https://doi.org/10.1073/pnas.1617945114

Wu, L.-Y., Stuart, F. M., Di Nicola, L., Heizler, M., Benvenuti, M., & Hu, R.-Z. (2019). Multi-aliquot method for determining (U+ Th)/He ages of hydrothermal hematite: Returning to Elba. *Chemical Geology*, *504*, 151–157. https://doi.org/10.1016/j.chemgeo.2018.11.005

Yund, R., Blanpied, M., Tullis, T., & Weeks, J. (1990). Amorphous material in high strain experimental fault gouges. *Journal of Geophysical Research*, *95*, 15589–15602. https://doi.org/10.1029/jb095ib10p15589